Volume 19 | Number 7 | 21 February 2017 | Pages 1011–1136

CrystEngComm

rsc.li/crystengcomm

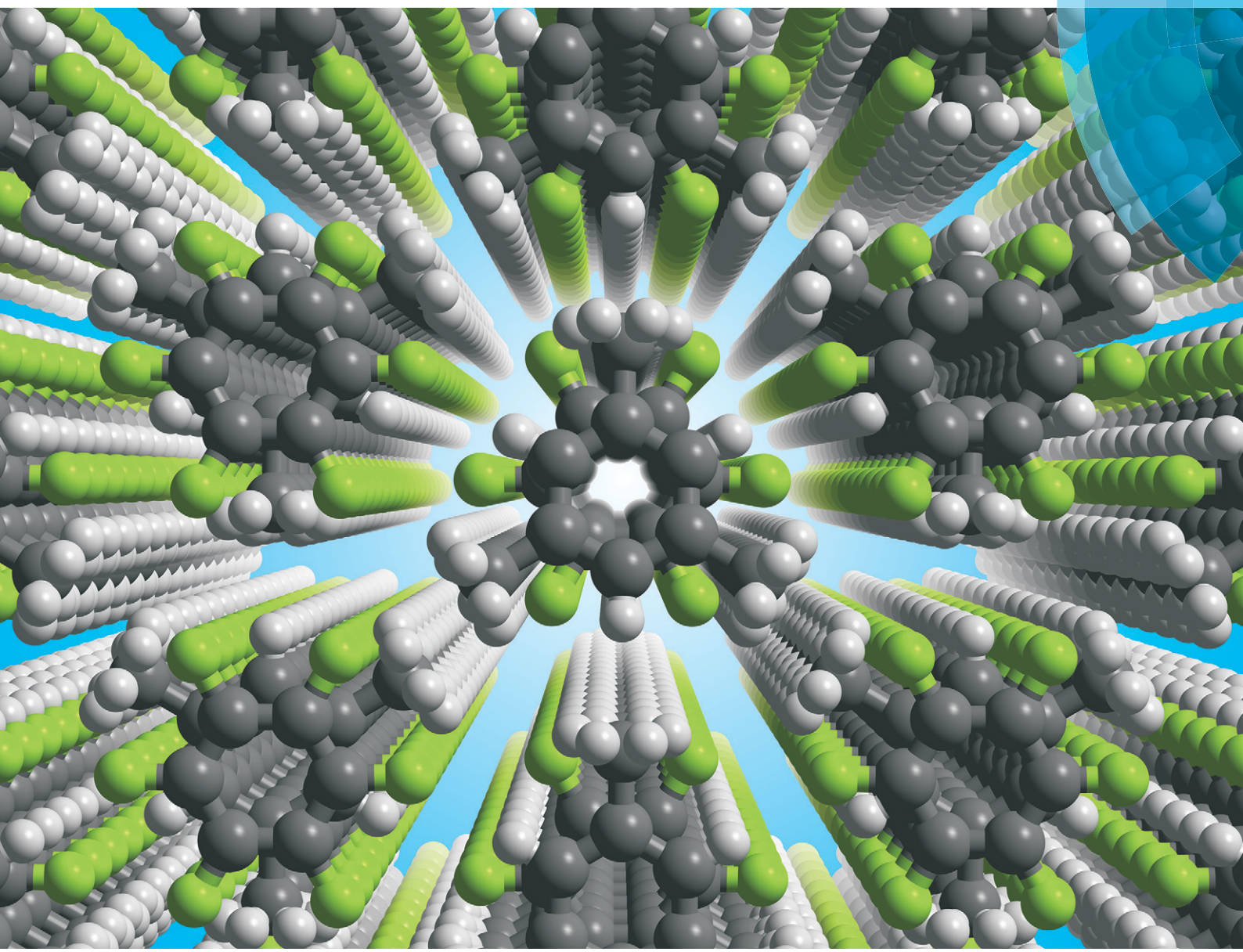

ROYAL SOCIETY OF CHEMISTRY

COMMUNICATION

Jeremy K. Cockcroft, Jeffrey H. Williams *et al.*

Investigation of the phase behaviour of the 1 : 1 adduct of mesitylene and hexafluorobenzene

CrystEngComm

COMMUNICATION

View Article Online
View Journal | View Issue

Cite this: *CrystEngComm*, 2017, **19**, 1019

Received 16th December 2016,
Accepted 20th January 2017

DOI: 10.1039/c6ce02581a

rsc.li/crystengcomm

Investigation of the phase behaviour of the 1 : 1 adduct of mesitylene and hexafluorobenzene†‡

Jeremy K. Cockcroft,*[a] Ronen E. Ghosh,[a] Jacob J. Shephard,[a] Anjali Singh[a] and Jeffrey H. Williams§*[b]

Variable temperature X-ray diffraction has been used to probe the structure and dynamics of the solid adducts of 1,3,5-trimethylbenzene (mesitylene) and hexafluorobenzene. PXRD patterns and DSC traces of near equimolar mixtures reveal two solid-state phase-transitions at 179.2 K and 111.0 K. The crystal structures of all three solid phases of this material have been solved by SXD. In contrast to previous studies on the adduct benzene–hexafluorobenzene, there is pairing of the mesitylene and hexafluorobenzene molecules in all three phases, each consisting of close-packed parallel columns of alternating $C_6H_3(CH_3)_3$ and C_6F_6 molecules packed face to face in a staggered conformation. Differences in structure between the phases illustrate the subtle interplay of quadrupole *versus* bond-dipole electrostatic interactions.

Introduction

Understanding weak non-covalent interactions is crucial for the prediction and control of organic solid-state structures.[1,2] Of particular interest is the design of organic co-crystals as alternatives to salts in the development of new materials in, for example, the pharmaceutical industry. For organic fluorine (*i.e.* bonded as C–F), there is a general consensus that fluorine rarely forms hydrogen bonds,[3,4] leading to questions about the nature of the interaction between C–F and H–C (or H_3C–) in the solid state.[5,6] The need to understand this type of weak interaction has become important in the health-care sector, where a variety of fluorinated active pharmaceutical ingredients (API's) have been developed, *e.g.* for use as antidepressants (fluoxetine, the API in Prozac), as cholesterol-lowering drugs (atorvastatin, the API in Lipitor), and as antibiotics (ciprofloxacin hydrochloride).[7]

One of the simplest organic co-crystals containing a molecule with a C–F bond and without hydrogen bonding is the 1 : 1 adduct of benzene (C_6H_6) and hexafluorobenzene (C_6F_6), first reported over 50 years ago.[8] C_6H_6 and C_6F_6 are liquids at room temperature, but the binary adduct is a solid. The structure of the lowest temperature phase was solved in 1991.[9] In addition to the complex with C_6H_6, C_6F_6 is known to form a series of 1 : 1 co-crystals with various methyl-substituted benzenes including mesitylene (1,3,5-$C_6H_3Me_3$),[10] hexamethylbenzene (C_6Me_6),[11,12] *p*-xylene (1,4-$C_6H_4Me_2$),[13] and durene (1,2,4,5-tetramethylbenzene).[14]

Our understanding of intermolecular interactions and cohesion in these materials has changed over time. Originally, they were thought to be so called 'charge-transfer solids'. It was thought that there was a donor–acceptor or π–π* bond between C_6H_6 and C_6F_6.[15–17] However, a transfer of charge and consequent molecular orbital changes are not supported by spectroscopy as the internal vibrations of the molecules in the adduct show only a small frequency shift when compared to those of the pure solids.[18,19]

An alternative model explaining cohesion in these 1 : 1 adducts is provided by studies of their charge distribution.[20,21] Given the lack of an overall dipole moment in C_6H_6, 1,3,5-$C_6H_3Me_3$, C_6Me_6, and C_6F_6, the first non-vanishing electrical moment for intermolecular interactions is the quadrupole moment. Experimental values of the quadrupole moment are available *via* the Buckingham technique of electric-field gradient-induced birefringence.[22–24] For C_6H_6, the value of the quadrupole is large and negative: -29.0×10^{-40} C m^2 and for C_6F_6 the quadrupole moment is large and positive: $+31.7 \times 10^{-40}$ C m^2.[23] The large negative value for C_6H_6, can be

[a] *Department of Chemistry, Christopher Ingold Laboratories, UCL, 20 Gordon Street, London WC1H 0AJ, UK. E-mail: j.k.cockcroft@ucl.ac.uk*
[b] *BIPM, Pavillon de Breteuil, 92312 Sèvres, France. E-mail: jeffreyhuw@hotmail.com*

† This paper is dedicated to Prof. David Buckingham FRS, after whom the CGS unit of the quadrupole moment is named.

‡ Electronic supplementary information (ESI) available: Additional experimental detail, crystallographic tables, and additional supporting figures are supplied. CIF files have been deposited at the Cambridge Crystallographic Data Centre with REFCODES 1518503 (phase I), 1518504 (phase II), and 1518505 (phase III). For ESI and crystallographic data in CIF or other electronic format see DOI: 10.1039/c6ce02581a

§ Current address: Montpellier, France.

interpreted with the familiar picture of delocalized charge above and below the plane of the C_6-ring. In contrast, due to the strong electronegativity of the fluorine atoms in C_6F_6, the electron charge density is contained in the plane of the C_6-ring and the sign of the quadrupole moment is positive. This makes C_6F_6 less susceptible to electrophilic attack than C_6H_6; an observation made and retained by every generation of organic chemist. The quadrupole moment of mesitylene is even more negative than that of benzene at -32.0×10^{-40} C m^2,[24] due to additional positive electric-charge residing on the $-CH_3$ groups. Thus, it is not surprising that mesitylene also forms a 1 : 1 adduct with hexafluorobenzene due to the favourable interaction of quadrupole moments in a similar way to C_6H_6:C_6F_6. In C_6H_6:C_6F_6 rotation of the rings occurs about the high symmetry axes of each component at higher temperatures;[9] by contrast the methyl groups of mesitylene can be expected to hinder such rotation. However, the methyl groups of mesitylene are free to rotate in order to optimize more specific and local charge interactions.

Results and discussion

Powder X-ray diffraction (PXRD) patterns collected in 10 K intervals reveal the presence of three solid phases below the melting point[25] (Fig. 1 and S1‡). In the PXRD patterns for the highest temperature phase I, the observed positions of the diffraction peaks are in good agreement with the unit cell and space-group symmetry determined by the pioneering 1970's single crystal diffraction (SXD) study,[10] Initially, indexing of the PXRD patterns of the intermediate phase II and the lowest temperature phase III were problematic due to some additional peaks with lower intensity.

The mean transition temperatures were found to be 111.0 K and 179.2 K (Fig. 2) from differential scanning calorimetry (DSC). The DSC data also shows that the overall composition of the sample changes when uncontained. C_6F_6 is more volatile and is readily lost from the sample leaving some residual $C_6H_3(CH_3)_3$. The residual $C_6H_3(CH_3)_3$, estimated at 9.3 wt% from its enthalpy of fusion, is clearly evident from the mean freezing/melting transition at 209.2 K.

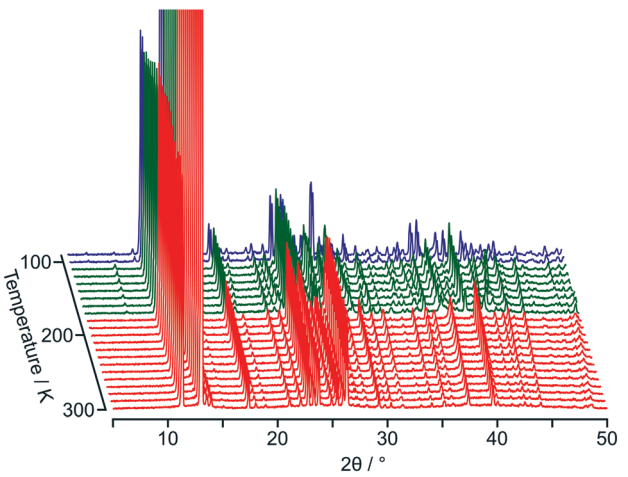

Fig. 1 PXRD data obtained on cooling a sample of $C_6H_3(CH_3)_3$:C_6F_6 from 300 K down to 90 K. Three distinct phases are observed: phase I (300 K to 180 K, data in red), phase II (170 K to 110 K, data in green), and phase III (100 K to 90 K, data in blue).

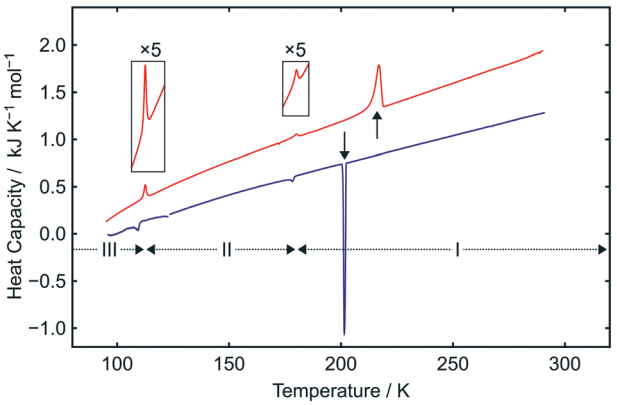

Fig. 2 DSC data obtained on cooling (blue curve) and heating (red curve) $C_6H_3(CH_3)_3$:C_6F_6. Two solid-state phase transitions and a freezing/melting transition are observed on cooling/heating. Similar results were obtained when the measurements were repeated. The exothermic and endothermic transitions indicated by vertical arrows correspond to the freezing and melting transitions, respectively, of a slight excess of $C_6H_3(CH_3)_3$ within the measured sample (see ESI‡ and Fig. S2). The heat capacity scale shown (exothermic down) is per mole of $C_6H_3(CH_3)_3$:C_6F_6.

In the present system, PXRD methods were found to be inappropriate for solving the crystal structure of any of the phases. X-ray diffraction measurements with a 2-D detector demonstrated that samples produced by quench cooling from the molten phase exhibit powder granularity (Fig. S3‡) and produce irreproducible intensities in the 1-D PXRD data (Fig. S4‡). Cooling through the phase transitions does not improve the quality of the PXRD samples as the crystallites survive the phase transitions.

The structures of phases I, II, and III were solved using SXD. A summary of the space-group symmetry and unit cells for each phase is given in Table 1. During the transition from phase I to II, single crystals are observed to undergo micro-domain twinning due to the change from orthorhombic to monoclinic symmetry but then revert back to orthorhombic symmetry in phase III, with loss of twinning and a doubling of the unit cell along a (Fig. S5‡). The crystals used in the SXD experiments visibly appeared macroscopically single throughout the cooling and heating cycles (Fig. S6‡). Selected crystallographic information is available in the ESI‡

Table 1 Comparative SXD data on the 3 phases of $C_6H_3(CH_3)_3$:C_6F_6

$C_6H_3(CH_3)_3$:C_6F_6	Phase I	Phase II	Phase III
Temperature/K	190	150	100
Space group	*Pbnm* (no. 62)	$P2_1/n$ (no. 14)	$Pb2_1a$ (no. 29)
a/Å	7.08543(18)	7.0737(3)	13.93854(8)
b/Å	15.3044(4)	15.2833(5)	15.18032(8)
c/Å	13.2959(4)	13.2104(4)	13.14822(7)
β/°	—	96.629(3)	—
Volume/*Z*/Å^3	360.45(2)	354.65(2)	347.756(8)

(Tables SI(a–f) to SIII(a–f) and Fig. S7); full-crystallographic information is available *via* deposited CIF files.

Comparative views of the crystal structure for each phase are shown in Fig. 3 and S8.‡ In all three phases, the molecules are arranged in columns formed of alternating C_6F_6 and $C_6H_3(CH_3)_3$ molecules arranged face to face. The columns themselves are approximately close-packed with six columns surrounding each column. It is noteworthy that in all three phases: (i) the molecules are slightly tilted with respect to the column axis (aligned to the crystallographic

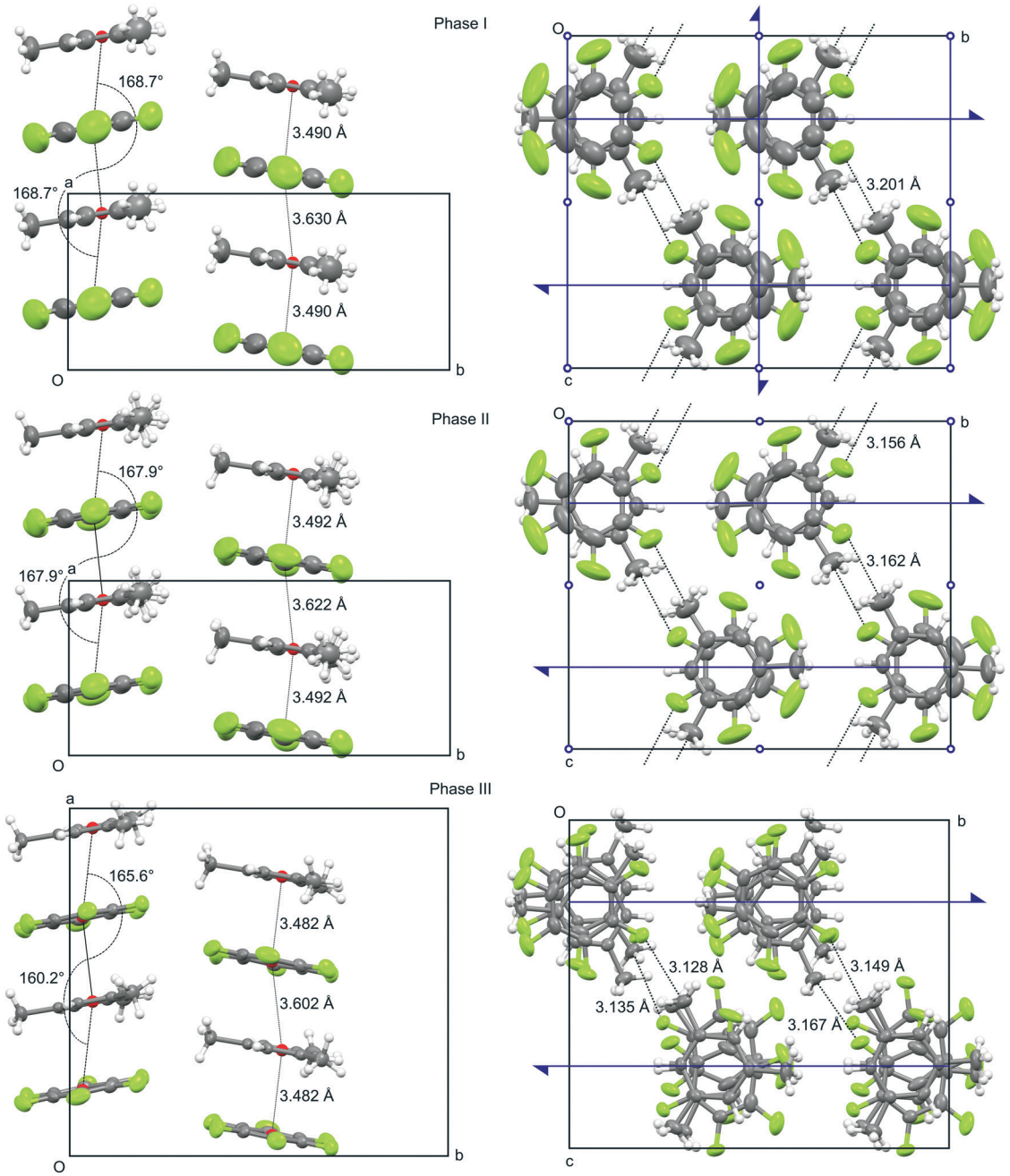

Fig. 3 Left: View of the crystal structures of $C_6H_3(CH_3)_3$:C_6F_6 seen down the *c*-axis for phase I (top), phase II (middle), and phase III (bottom) showing the distances between ring centroids shown in red (s.u. equal to 0.003 Å) and the angles formed by lines joining the ring centroids (s.u. equal to 0.1°). In phase III, there are two crystallography distinct pairs of molecules: an additional set of interplanar distances (3.482(3) Å and 3.648(3) Å) and corresponding angles (155.6(1)° and 168.3(1)°) were calculated from the second pair (not seen in bottom-left figure). The increase in the dynamical motion of the molecules with increasing temperature is evidenced by the size of the 'thermal' ellipsoids; mean atomic-displacement parameters are shown as ellipsoids at the 50% probability level. C, F, and H atoms types are drawn in grey, green, and white, respectively. Right: Views seen down the *a*-axis for phase I (top), phase II (middle), and phase III (bottom) showing: (i) the staggered arrangement of the rings within a column; (ii) the C–F···CH_3–C interactions that bind adjacent columns together; and (iii) selective symmetry elements present in each crystal structure (blue). Additional views of the structures are in Fig. S8 and S9.‡

a-axis); (ii) they exist as distinct pairs with alternating ring-to-ring centroid distances of about 3.5 Å and 3.6 Å; (iii) within a column, the C_6F_6 and $C_6H_3(CH_3)_3$ rings are staggered, similar to the behaviour of the rings observed in phase IV of C_6H_6:C_6F_6;[9] and (iv) that the binding between adjacent columns occurs *via* weak electrostatic interactions between the C–F bond dipole moment in one column and the H_3C–C bond dipole moment in neighbouring columns. The importance of the bond-dipole–bond-dipole interactions in stabilizing the inter-columnar interactions in these adducts is also seen in the structure of solid fluorobenzenes.[7]

The variation in the influence of this inter-columnar interaction as a function of temperature gives rise to the three solid phases. Positions of all hydrogen atoms in mesitylene can be located by SXD in all three phases of $C_6H_3(CH_3)_3$:C_6F_6. In phase I, all three $-CH_3$ groups of mesitylene appear crystallographically disordered; in phase II, two of the $-CH_3$ groups are disordered but one is ordered; and in phase III, all three of the $-CH_3$ groups are ordered.

The directionality of the C–CH_3 groups toward F atoms is particularly informative in interpreting the cohesive intermolecular interactions. In all phases, two of the three $-CH_3$ groups are aligned directly at F atoms ($\angle$F$\cdots H_3$C–C is 176.7(2)° in phase I; 171.9(2)° and 177.8(2)° in phase II; and 168.4(2)°, 169.7(2)°, 170.7(2)°, and 172.9(2)° in phase III). The measured near linear arrangement of the positions of the heavy atoms in F$\cdots H_3$C–C suggests an inter-columnar interaction that has little dependence on the orientation of the H atoms of the methyl group about the H_3C–C bond. This electrostatic interaction is sufficiently powerful to pin down two of the F atoms of an adjacent C_6F_6 ring and explains the observed thermal motion of the C_6F_6 ring as evidenced by the large variation in anisotropic displacement ellipsoids for the F atoms in all three phases (Fig. 3). The third methyl group in mesitylene is unable to align directly with any F atom and in phase II its H atoms adopt a fixed position resulting in a slight displacement of adjacent columns parallel to the column axis, and a monoclinic distortion of the structure (Fig. S8 and S9‡). Further ordering of the methyl groups occurs on cooling to phase III as further optimization of the inter-column interactions takes place. In all three phases, the net in-plane librational motion of the rigid C_6F_6 molecule is not about its centre of mass in contrast to the averaged librational cloud of the $C_6H_3(CH_3)_3$ molecule, where the rotational axis is about its centre.

Determination of the structures of each phase enabled lattice parameters to be obtained as a function of temperature from the PXRD data. The volume change with temperature (Fig. 4) shows that $C_6H_3(CH_3)_3$:C_6F_6 behaves like a typical covalent solid: the volume per dimeric unit increases by 8.7% on heating from 90 K to 300 K.

The symmetry of the transition from orthorhombic phase I to monoclinic phase II involves a group sub-group relationship, as the space group $P2_1/n$ is a maximal non-isomorphic subgroup of *Pbnm*. The inversion symmetry is conserved along with the 2_1 screw axis along **b** and the *n*-glide plane

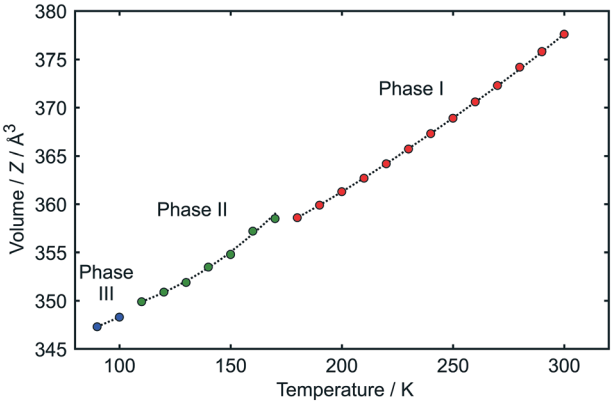

Fig. 4 Volume per $C_6H_3(CH_3)_3$:C_6F_6 as a function of temperature as derived from whole pattern fitting of the data shown in Fig. 1. The variation of individual unit-cell parameters with temperature is given in Table S4 and is shown in Fig. S10.‡

perpendicular to **b** (Fig. 3, right). In order to compare the structures at different temperatures, standard crystallographic space-group settings were used for phase II (*i.e. b*-axis unique with a centrosymmetric origin) and, consequently, non-standard settings were required for phases I and III (see ESI‡). In phase I, the molecules are bisected by the mirror plane in space group *Pbnm* (Fig. S7‡), which is a non-standard setting of *Pnma*. In phase III, a non-standard setting of $Pca2_1$ is used, namely $Pb2_1a$, together with a non-standard shift in origin due to the doubling of the unit cell (Table S3a‡): the transition from phase II to phase III involves a loss of inversion symmetry and the only symmetry element that is maintained throughout all three phases is the 2_1 screw axis along **b**. Given that $Pb2_1a$ is a polar space group, this indicates a ferroelectric transition from phase II to III.

Experimental

Samples of the $C_6H_3(CH_3)_3$:C_6F_6 complex were prepared by adding liquid mesitylene and hexafluorobenzene together in a 1 : 1 molar ratio. PXRD measurements were made using a Stoe Stadi-P diffractometer. SXD measurements were made using an Agilent SuperNova diffractometer. DSC measurements were made using a PerkinElmer DSC8000 equipped with a liquid N_2 cold stage operating down to 93 K. Further details of all experiments are available in the ESI.‡

Conclusions

Using X-ray diffraction, the structure of each of the three phases that exist in the solid adduct formed between 1,3,5-trimethylbenzene and hexafluorobenzene in the temperature range 90 K to 300 K have been determined. Simple ideas of molecular electrostatics, based on the observed values of the molecular quadrupole moments, allow us to explain the ordering of molecules within the close-packed stacked columns present in the structures of all three phases; and the concept of a bond dipole moment permits an explanation of the

shorter-range inter-columnar interactions. These interactions become increasingly constrained as the temperature is decreased and are the origin of the phase-transitions. Current calculations on organic crystal structures[26] are, as yet, unable to predict thermal motion, and so identify instability. It is the delicate balance between intermolecular forces and thermal motion which determines the presence of any phase transition.

Acknowledgements

We acknowledge financial support from the EPSRC for funding the X-ray diffractometers (grant reference EP/K03930X/1). We thank Dr Christoph Salzmann for use of the Royal Society funded DSC calorimeter and Martin Vickers for PXRD support.

References

1 J. D. Dunitz and A. Gavezzotti, *Chem. Soc. Rev.*, 2009, **38**, 2622–2633.
2 G. R. Desiraju, *J. Am. Chem. Soc.*, 2013, **135**, 9952–9967.
3 P. Panini and D. Chopra, in *Hydrogen Bonded Supramolecular Structures, Lecture Notes in Chemistry*, ed. Z. Li and L. Wu, Springer-Verlag, 2015, ch. 2, vol. 87, pp. 37–67.
4 A. Gavezzotti and L. L. Presti, *Cryst. Growth Des.*, 2016, **16**, 2952–2962.
5 J. A. K. Howard, V. J. Hoy, D. O'Hagan and G. T. Smith, *Tetrahedron*, 1996, **52**, 12613–12622.
6 V. R. Thalladi, H.-C. Weiss, D. Bläser, R. Boese, A. Nangia and G. R. Desiraju, *J. Am. Chem. Soc.*, 1998, **120**, 8702–8710.
7 K. Müller, C. Faeh and F. Diederich, *Science*, 2007, **317**, 1881–1886.
8 C. R. Patrick and G. S. Prosser, *Nature*, 1960, **187**, 1021.
9 J. H. Williams, J. K. Cockcroft and A. N. Fitch, *Angew. Chem., Int. Ed. Engl.*, 1992, **31**, 1655–1657.
10 T. Dahl, *Acta Chem. Scand.*, 1971, **25**, 1031–1039.
11 T. Dahl, *Acta Chem. Scand.*, 1972, **26**, 1569–1575.
12 T. Dahl, *Acta Chem. Scand.*, 1973, **27**, 995–1003.
13 T. Dahl, *Acta Chem. Scand., Ser. A*, 1975, **29**, 170–174.
14 T. Dahl, *Acta Chem. Scand., Ser. A*, 1975, **29**, 699–705.
15 D. F. R. Gilson and C. A. McDowell, *Can. J. Chem.*, 1966, **44**, 945–952.
16 T. Dahl, *Acta Chem. Scand., Ser. A*, 1988, **42**, 1–7.
17 J. H. Williams, *Acc. Chem. Res.*, 1993, **26**, 593–598.
18 J. H. Williams, *Mol. Phys.*, 1991, **73**, 99–112.
19 J. H. Williams, *Chem. Phys.*, 1993, **172**, 171–186.
20 N. M. D. Brown and F. L. Swinton, *J. Chem. Soc., Chem. Commun.*, 1974, 770–771.
21 J. Hernandez-Trujillo, M. Costas and A. Vela, *J. Chem. Soc., Faraday Trans.*, 1993, **89**, 2441–2443.
22 A. D. Buckingham, *J. Chem. Phys.*, 1959, **30**, 1580–1585.
23 M. R. Battaglia, A. D. Buckingham and J. H. Williams, *Chem. Phys. Lett.*, 1981, **78**, 421–423.
24 J. Vrbancich and G. D. L. Richie, *J. Chem. Soc., Faraday Trans. 2*, 1980, **76**, 648–659.
25 W. A. Duncan and F. L. Swinton, *Trans. Faraday Soc.*, 1966, 1082–1089.
26 A. M. Reilly, *et al.*, *Acta Crystallogr., Sect. B: Struct. Sci., Cryst. Eng. Mater.*, 2016, **72**, 439–459.